J. Fluid Mech. (1995), *vol.* 289, *pp.* 159–177

The evolution of a localized vortex disturbance in external shear flows. Part 1. Theoretical considerations and preliminary experimental results

By VLADIMIR LEVINSKI AND JACOB COHEN
Faculty of Aerospace Engineering, Technion – Israel Institute of Technology, Haifa 32000, Israel

(Received 21 April 1994 and in revised form 21 November 1994)

The evolution of a finite-amplitude three-dimensional localized disturbance embedded in external shear flows is addressed. Using the fluid impulse integral as a characteristic of such a disturbance, the Euler vorticity equation is integrated analytically, and a system of linear equations describing the temporal evolution of the three components of the fluid impulse is obtained. Analysis of this system of equations shows that inviscid plane parallel flows as well as high Reynolds number two-dimensional boundary layers are always unstable to small localized disturbances, a typical dimension of which is much smaller than a dimensional length scale corresponding to an $O(1)$ change of the external velocity. Since the integral character of the fluid impulse is insensitive to the details of the flow, universal properties are obtained. The analysis predicts that the growing vortex disturbance will be inclined at 45° to the external flow direction, in a plane normal to the transverse axis. This prediction agrees with previous experimental observations concerning the growth of hairpin vortices in laminar and turbulent boundary layers. In order to demonstrate the potential of this approach, it is applied to Taylor–Couette flow, which has additional dynamical effects owing to rotation. Accordingly, a new instability criterion associated with three-dimensional localized disturbances is found. The validity of this criterion is supported by our experimental results.

1. Introduction

The purpose of the present work is to derive a general model which is capable of characterizing the evolution of three-dimensional localized disturbances in shear flows. The original motivation for this investigation was to explain the growth of hairpin vortices in turbulent boundary layers. However, as will be shown, this formalism can be applied to several kinds of shear flows. In fact, when applied to the Taylor–Couette flow, a new instability criterion associated with finite-amplitude three-dimensional localized disturbances emerged. As predicted by this criterion and supported by our experimental results, the flow is unstable to such disturbances over a range of parameters, while the flow is expected to be stable according to Landau & Lifshitz (1959).

The assumptions used in the model are based on geometrical characteristics of the hairpin vortices found in a series of experiments which followed the pioneering work of Kline *et al.* (1967). They were the first to observe the well-organized streaky structure in the near-wall region of a turbulent boundary layer. A brief summary of papers relevant to this subject can be found in the article by Head & Bandyopadhyay (1981). By using a sophisticated flow visualization procedure they were able to

conclude that at Reynolds numbers, $Re_\theta > 200$, the layer appears to consist very largely of elongated hairpin vortices, originating in the wall region and extending throughout a substantial part of the boundary layer or beyond it. These vortices were found to have a characteristic inclination of 45° and remain identifiable even at high Reynolds numbers of the order of $Re_\theta \approx 10000$. At low Reynolds numbers, $Re_\theta < 800$, the hairpin vortices are much less elongated and are better described as horseshoe vortices or vortex loops. Hairpin vortices were artificially generated in a laminar boundary layer by Acarlar & Smith (1987*a*, *b*). Comparison of their results with the vortical structures observed in turbulent boundary layers show striking similarities with regard to the details of the vortical structures which consist of a head and counter-rotating legs inclined at 45° to the main flow direction. Using numerical simulations, Moin & Kim (1985) reproduced all the features of hairpin vortices in turbulent channel flow. Recently, Hagen & Kurosaka (1993) studied the interiors of these structures and discovered the existence of cross-flow transport inside the cores of the hairpin legs, having a corewise velocity of 0.75 of the free stream velocity. In fact, this transport can explain the mechanism of turbulent mixing in boundary layers.

The evolution of localized disturbances cannot be explained solely by a two-dimensional instability mechanism. This was recognized by Landahl (1975), who pointed out that the non-dispersive advective part of an initial inviscid three-dimensional disturbance, which travels at the local mean velocity of the fluid, has a very different character than the corresponding part of a two-dimensional disturbance. He noted that the solution for any three-dimensional disturbance contains a non-vanishing component in the vertical (normal to the wall) direction, which he termed the 'liftup' effect. If there is a mean shear, the integrated effect of this 'liftup' mechanism creates a streamwise disturbance velocity which does not disappear for long times. Further studies, using theoretical models, direct numerical simulations and analysis of the linearized Navier–Stokes equations, by Russell & Landahl (1984), Henningson (1988), Breuer & Haritonidis (1990), Breuer & Landahl (1990), Gustavsson (1991) and Henningson, Lundbladh & Johansson (1993), have shown that three-dimensionality plays a key role and allows for algebraic growth of the normal vorticity through the linear liftup mechanism. This growth primarily generates elongated structures in the streamwise direction (much longer than the boundary layer thickness), forming an inclined shear layer which is tilted, stretched and intensified by the mean shear as it travels downstream.

Orszag & Patera (1983) showed that, alone, neither the tilting of the mean vorticity by the perturbation's velocity field nor the advection and stretching of the perturbation vorticity by the mean flow, can ever lead to exponential growth of the initial disturbance. In their review article, Bayly, Orszag & Herbert (1988) argued that the three-dimensional instability results from a delicate balance between the stretching of old perturbation vorticity and the perpetual generation of new vorticity by the tilting of the basic flow vorticity. This argument is supported by the study of the elliptical instability (Bayly 1986) and by the study of the transient growth of optimal perturbations in constant-shear flows (Farrell & Ioannou 1993).

The present approach follows some of the ideas described above. However, it focuses on the evolution of localized disturbances for which all dimensions are of the same order and much smaller than the boundary layer thickness. In order to account for the integrated 'liftup' effect we shall follow the evolution in time of the fluid impulse integral, $\boldsymbol{P}$, defined as

$$\boldsymbol{P} = \frac{1}{2}\int \boldsymbol{x} \times \boldsymbol{\omega}(\boldsymbol{x})\, \mathrm{d}V, \tag{1}$$

where the bold type indicates vector character, $\boldsymbol{x}$ is the position vector, $\boldsymbol{\omega}$ is the vorticity vector, $\mathrm{d}V$ is a volume element and the integral is taken over the whole fluid.

The attraction of the fluid impulse is that it is an invariant of self-induced motion in unbounded three-dimensional flow (Batchelor 1967). Consequently, the evolution of the fluid impulse for a localized disturbance is characterized by a linear equation, even though the motion of the vortical localized disturbance is governed by strong nonlinear effects. The integral character of the fluid impulse prevents us from knowing the details of the evolution in time and redistribution of the vorticity enclosed within the disturbed vortical region. However, this insensitivity to the details of the flow leads us to expect some universal properties. The fluid impulse is also a very powerful tool if one is interested in the asymptotic behaviour of the velocity and pressure in the far field (Rott & Cantwell 1993), and in the evolution of the confined vortical region as a whole. In previous works Roberts (1972) and then Grigoriev, Levinski & Yanenko (1982) used the fluid impulse to describe the time evolution of interacting vortices embedded in a potential flow.

In what follows we shall explain the space and time evolution of such localized vortices surrounded by external shear flows. In accordance with the above-mentioned experimental observations, we assume that the effect of the Reynolds number is secondary and the only role of the wall is to generate the initial disturbance, the dimensions of which are much smaller than a typical scale representing the velocity gradient of the external flow. Consequently we shall follow the evolution of the fluid impulse in an unbounded inviscid flow and take advantage of its properties.

2. Analysis

The three-dimensional vorticity equation for an incompressible and inviscid flow is given by

$$\frac{\partial \boldsymbol{\Omega}_T}{\partial t}+(\boldsymbol{U}_T\cdot\boldsymbol{\nabla})\,\boldsymbol{\Omega}_T-(\boldsymbol{\Omega}_T\cdot\boldsymbol{\nabla})\,\boldsymbol{U}_T=0, \tag{2}$$

where the total velocity vector $\boldsymbol{U}_T$ and the total vorticity vector $\boldsymbol{\Omega}_T$ are related by $\boldsymbol{\Omega}_T=\boldsymbol{\nabla}\times\boldsymbol{U}_T$. We consider these vectors as being the sum of two contributions: the external shear field (or 'background field') in which $\boldsymbol{\Omega}=\boldsymbol{\nabla}\times\boldsymbol{U}$, and a finite-amplitude disturbed field in which $\boldsymbol{\omega}=\boldsymbol{\nabla}\times\boldsymbol{u}$. Thus, the total velocity and vorticity vectors can be written as

$$\boldsymbol{U}_T=\boldsymbol{U}+\boldsymbol{u} \quad \text{and} \quad \boldsymbol{\Omega}_T=\boldsymbol{\Omega}+\boldsymbol{\omega}. \tag{3}$$

When (3) is substituted into (2) and the undisturbed equation for the external flow is subtracted we obtain

$$\frac{\partial \boldsymbol{\omega}}{\partial t}+(\boldsymbol{U}\cdot\boldsymbol{\nabla})\,\boldsymbol{\omega}-(\boldsymbol{\omega}\cdot\boldsymbol{\nabla})\,\boldsymbol{U}+(\boldsymbol{u}\cdot\boldsymbol{\nabla})\,\boldsymbol{\Omega}-(\boldsymbol{\Omega}\cdot\boldsymbol{\nabla})\,\boldsymbol{u}+(\boldsymbol{u}\cdot\boldsymbol{\nabla})\,\boldsymbol{\omega}-(\boldsymbol{\omega}\cdot\boldsymbol{\nabla})\,\boldsymbol{u}=0, \tag{4}$$

for which the undisturbed external flow field is assumed to be a known solution of (2). The disturbed vorticity at the initial time t_0, is given by

$$\boldsymbol{\omega}(\boldsymbol{x}, t=t_0)=\boldsymbol{\omega}_0(\boldsymbol{x}), \tag{5}$$

and it is assumed that $\boldsymbol{\omega}_0$ is confined to a very small region, a typical size of which is $\delta \ll \Delta$, where Δ is a dimensional length scale corresponding to an $O(1)$ change of the external velocity.

In a previous paper, Aref & Flinchem (1984) used the fraction $\delta/\Delta \ll 1$ as a small parameter in order to estimate the relative magnitudes of the terms describing the interaction between the vortex disturbance and the external flow in (4). In their analysis the vortex disturbance was taken as a quasi-two-dimensional slender tube of diameter δ, so that variations along the tube were much smaller than those across it. By comparing orders, they showed that the second term in (4) is the most important one. This term describes the advection of the vortex tube by the background velocity field. Physically, the dominance of this term is attributed to the fact that a typical length scale along the tube is relatively long, of $O(\Delta)$, and consequently the corresponding shear of the external flow becomes significant.

In the case described in this paper, the disturbed vorticity is assumed to be confined to a small region, of length $O(\delta)$ in all directions. Therefore, the shear across any direction of the disturbed region is at least $O(\delta/\Delta)$ smaller than the corresponding shear along the tube in the case described above. Since the advection of the small disturbed region as a whole is not of interest, we use a Galilean frame, moving with the disturbance, instead of the laboratory frame. Accordingly, the origin of the coordinate system is redefined to be some point within the initially disturbed region so that $\boldsymbol{U}(0) = 0$.

Taking advantage of the smallness of the disturbed region, the external velocity and vorticity fields around the origin are approximated by Taylor series expansions. Using the magnitude of the background shear $|\boldsymbol{\Omega}|$ and the length scale Δ as the appropriate scales representing the external flow, the Taylor series expansions are given by

$$U_i(\boldsymbol{x}) = \sum_{j=1}^{3} \frac{\partial U_i(0)}{\partial x_j} x_j + O\left(|\boldsymbol{\Omega}(0)|\,|\boldsymbol{x}| \cdot \left(\frac{|\boldsymbol{x}|}{\Delta}\right)\right), \tag{6}$$

and

$$\Omega_i(\boldsymbol{x}) = \Omega_i(0) + O\left(|\boldsymbol{\Omega}(0)| \cdot \left(\frac{|\boldsymbol{x}|}{\Delta}\right)\right), \tag{7}$$

where the leading term in (6) is $O(|\boldsymbol{\Omega}(0)|\,|\boldsymbol{x}|)$ and $|\boldsymbol{x}|/\Delta \ll 1$.

The magnitude of the fluid impulse integral $|\boldsymbol{P}|$ and the length δ are chosen as representative scales of the disturbed field. Accordingly, typical magnitudes of the disturbed vorticity and velocity are $|\boldsymbol{\omega}| \sim |\boldsymbol{P}|/\delta^4$ and $|\boldsymbol{u}| \sim |\boldsymbol{P}|/\delta^3$, respectively, while the magnitude of the external velocity within and in the vicinity of the disturbed region is $|\boldsymbol{U}| \sim |\boldsymbol{\Omega}|\delta$.

Using these scales, the magnitudes of the terms in (4) describing the interaction between the vortex disturbance and the external flow are estimated to be

$$|(\boldsymbol{U}\cdot\boldsymbol{\nabla})\boldsymbol{\omega}|, \quad |(\boldsymbol{\omega}\cdot\boldsymbol{\nabla})\boldsymbol{U}|, \quad |(\boldsymbol{\Omega}\cdot\boldsymbol{\nabla})\boldsymbol{u}| \sim O\left(\frac{|\boldsymbol{\Omega}|\,|\boldsymbol{P}|}{\delta^4}\right), \tag{8}$$

and

$$|(\boldsymbol{u}\cdot\boldsymbol{\nabla})\boldsymbol{\Omega}| \sim O\left(\frac{|\boldsymbol{\Omega}|\,|\boldsymbol{P}|}{\delta^4}\frac{\delta}{\Delta}\right). \tag{9}$$

Since the fourth term in (4) is $O(\delta/\Delta)$ smaller than the rest, it will be neglected. Thus, to leading order the vorticity equation is reduced to

$$\frac{\partial \boldsymbol{\omega}}{\partial t} + (\boldsymbol{U}\cdot\boldsymbol{\nabla})\boldsymbol{\omega} - (\boldsymbol{\omega}\cdot\boldsymbol{\nabla})\boldsymbol{U} - (\boldsymbol{\Omega}\cdot\boldsymbol{\nabla})\boldsymbol{u} + (\boldsymbol{u}\cdot\boldsymbol{\nabla})\boldsymbol{\omega} - (\boldsymbol{\omega}\cdot\boldsymbol{\nabla})\boldsymbol{u} = \boldsymbol{0}. \tag{10}$$

The simplified vorticity equation (10) and the simplified expressions for the external velocity and vorticity fields given by (6) and (7) are a direct consequence of the

assumption that $\delta/\Delta \ll 1$. From here onwards we shall regard this ratio as being infinitesimally small so that the initially embedded vorticity region is in fact surrounded by an infinite field having a constant-velocity shear.

In order to study the development of the initial localized vorticity disturbance, we follow the time evolution of the fluid impulse, i.e.

$$\frac{\mathrm{d}\boldsymbol{P}}{\mathrm{d}t} = \frac{1}{2}\int \boldsymbol{x} \times \frac{\partial \boldsymbol{\omega}(\boldsymbol{x}, t)}{\partial t}\,\mathrm{d}V, \tag{11}$$

where the time derivative of $\boldsymbol{\omega}(\boldsymbol{x}, t)$ is determined from (10). It should be noted that for a bounded vorticity field, the resultant fluid impulse is invariant under a Galilean transformation.

Since the time evolution of the fluid impulse is an integral over the whole volume, we must first verify that most of the contribution to this integral comes from the localized disturbed region; otherwise, the use of Taylor series expansions and the neglect of the fourth term in (4) are not justified. According to (10), the vorticity generated during a typical time scale of $O(1/|\boldsymbol{\Omega}|)$, is of the order of $|\boldsymbol{\omega}_0|$. This vorticity, except for the part generated via the fourth term in (10), is confined to the disturbed region. Therefore, its contribution to the evolution of the fluid impulse (11) is of the order of $|\boldsymbol{P}| \sim O(|\boldsymbol{\omega}_0|\delta^4) \sim O(|\boldsymbol{P}_0|)$, where the subscript 0 indicates the evaluation of all quantities at time t_0.

The only term which might generate vorticity away from the localized region is the fourth term in (10), which describes the stretching of the external vorticity by the velocity field induced by the disturbance. The velocity field induced by the localized vortex disturbance at locations far from it is given by

$$\boldsymbol{u}(\boldsymbol{x}) \sim \frac{1}{8\pi}\boldsymbol{\nabla}\left(\boldsymbol{\nabla}\frac{1}{|\boldsymbol{x}|}\cdot\int \boldsymbol{x}' \times \boldsymbol{\omega}(\boldsymbol{x}')\,\mathrm{d}V'\right) + O\left(\frac{1}{|\boldsymbol{x}|^4}\right), \tag{12}$$

where $|\boldsymbol{x}| \to \infty$ (Batchelor 1967). Substituting (1) into (12) with $|\boldsymbol{x}| \gg \delta$ and $t = t_0$ we obtain

$$\boldsymbol{u}_0(\boldsymbol{x}) \sim -\frac{1}{4\pi}\left[\frac{\boldsymbol{P}_0}{|\boldsymbol{x}|^3} - \frac{3(\boldsymbol{P}_0\cdot\boldsymbol{x})\,\boldsymbol{x}}{|\boldsymbol{x}|^5}\right] + O\left(\frac{1}{|\boldsymbol{x}|^4}\right). \tag{13}$$

Thus, although the far-field vorticity generated by the self-induced velocity field (the fourth term in (10)) is very small, of $O(|\boldsymbol{\omega}_0|\delta^4/|\boldsymbol{x}|^4)$, its integrated contribution over some volume, including the far field ($|\boldsymbol{x}| \gg \delta$) and excluding the disturbed region, is of the same order as that of the near field, i.e. $O(|\boldsymbol{P}_0|)$. Furthermore, since the vorticity diminishes in magnitude as $|\boldsymbol{x}|^{-4}$, the integral (11) is not absolutely convergent and depends on how the integral is taken.

In order to overcome this difficulty we subdivide the velocity and vorticity fields into two parts as follows:

$$\boldsymbol{\omega} = \boldsymbol{\omega}^I + \boldsymbol{\omega}^{II} \quad \text{and} \quad \boldsymbol{u} = \boldsymbol{u}^I + \boldsymbol{u}^{II}, \tag{14}$$

so that $\boldsymbol{\omega}^{I,II} = \boldsymbol{\nabla} \times \boldsymbol{u}^{I,II}$. Therefore, for each part we require that

$$\boldsymbol{\nabla}\cdot\boldsymbol{\omega}^I = \boldsymbol{\nabla}\cdot\boldsymbol{\omega}^{II} = 0. \tag{15}$$

Consequently, the disturbed velocity fields generated by the vorticity fields $\boldsymbol{\omega}^{I,II}$ are given by

$$\boldsymbol{u}^{I,II}(\boldsymbol{x}, t) = -\frac{1}{4\pi}\int \frac{(\boldsymbol{x}-\boldsymbol{x}') \times \boldsymbol{\omega}^{I,II}(\boldsymbol{x}', t)}{|\boldsymbol{x}-\boldsymbol{x}'|^3}\,\mathrm{d}V'. \tag{16}$$

The first part, indicated by the superscript I, is regarded by us as the one associated with the concentrated vorticity confined within and in the vicinity of the initially disturbed region, whereas the second part, indicated by the superscript II, is associated with the far-field vorticity generated via the fourth term of (10). Accordingly, we set the initial distribution of the vorticity fields as

$$\omega^I(x, t = t_0) = \omega_0(x) \quad \text{and} \quad \omega^{II}(x, t = t_0) = 0, \tag{17}$$

and intend to follow the evolution of $\omega^I(x, t)$. We note that the fourth term in (10) can be decomposed into $(\Omega \cdot \nabla) u = -\Omega \times \omega + \nabla(\Omega \cdot u)$, in which only the latter part is responsible for generating far-field vorticity. Therefore we introduce the function $\Psi(x, t)$, chosen so that away from the disturbed region $\Psi(x, t) = \Omega \cdot u^I$, and by using (12) or (13), its asymptotic behaviour is given by

$$\Psi = -\frac{1}{4\pi}\left[\frac{(\Omega \cdot p)}{|x|^3} - \frac{3(\Omega \cdot x)(p \cdot x)}{|x|^5}\right] + \text{higher-order terms}, \tag{18}$$

where p is the fluid impulse corresponding to ω^I, i.e.

$$p = \frac{1}{2}\int x \times \omega^I(x)\, \mathrm{d}V. \tag{19}$$

The corresponding system of vorticity equations is given by

$$\frac{\partial \omega^I}{\partial t} + (U \cdot \nabla)\omega^I - (\omega^I \cdot \nabla) U - (\Omega \cdot \nabla) u^I + (u \cdot \nabla)\omega - (\omega \cdot \nabla) u + \nabla \Psi = 0, \tag{20}$$

$$\frac{\partial \omega^{II}}{\partial t} + (U \cdot \nabla)\omega^{II} - (\omega^{II} \cdot \nabla) U - (\Omega \cdot \nabla) u^{II} - \nabla \Psi = 0, \tag{21}$$

for which the sum of the two equations, together with the sum of the initial conditions given in (17), yields the original problem. It should be noted that without loss of generality, ω^{II} can be chosen arbitrarily, provided that $\nabla \cdot \omega^{II} = 0$.

In order to ensure this condition at all times (note that at $t = t_0$ this condition is satisfied, (17)), we apply the operator $(\nabla \cdot)$ to (20) and (21), and use (15) and (7)† to obtain that $\Delta \Psi(x, t) = 0$ everywhere. Thus, Ψ must be a piecewise-continuous harmonic function which asymptotically vanishes at a rate given by (18). We subdivide all space into two regions, inside and outside a spherical domain of radius $R \geqslant \delta$, enclosing the disturbance. We construct Ψ as being composed of two functions, Ψ_o and Ψ_i, corresponding to $|x|$ greater than and smaller than $R \geqslant \delta$, respectively. The outer function, Ψ_o, is set to be equal to the leading term of (18), whereas the inner function, Ψ_i, is determined by solving the Neumann problem for which $\Delta \Psi_i(x, t) = 0$ and $n \cdot \partial \Psi_i / \partial n = n \cdot \partial \Psi_o / \partial n$ on the spherical boundary $|x| = R$, where n is the unit vector normal to boundary surface. Accordingly, the expression for Ψ_i is given by

$$\Psi_i = \frac{3}{8\pi R^5}[(\Omega \cdot p)|x|^2 - 3(\Omega \cdot x)(p \cdot x)]. \tag{22}$$

Since $\nabla \Psi$ cancels the leading terms of the vorticity generated via the fourth term in (20) the asymptotic behaviour of ω^I is given by

$$|\omega^I(x, t)| \sim O\left(\frac{1}{|x|^5}\right) \quad \text{for} \quad |x| \gg \delta. \tag{23}$$

† The approximation (7) is necessary only because the fourth term in (4) has been dropped.

Consequently, the fluid impulse integral (19) is absolutely convergent and the resultant integral is not dependent on the way in which the volume of the integration is allowed to tend to infinity. For convenience we use a spherical volume with a radius $R_1 \to \infty$ so that the time evolution of $\boldsymbol{p}$ can be evaluated from

$$\frac{\mathrm{d}\boldsymbol{p}}{\mathrm{d}t} = \tfrac{1}{2} \lim_{R_1 \to \infty} \int_{|\boldsymbol{x}| \leqslant R_1} \boldsymbol{x} \times \frac{\partial \boldsymbol{\omega}^I(\boldsymbol{x}, t)}{\partial t} \mathrm{d}V. \tag{24}$$

Substitution of (20) into (24) yields

$$\frac{\mathrm{d}\boldsymbol{p}}{\mathrm{d}t} = -\tfrac{1}{2} \lim_{R_1 \to \infty} \int_{|\boldsymbol{x}| \leqslant R_1} \boldsymbol{x} \times [(\boldsymbol{U} \cdot \nabla)\boldsymbol{\omega}^I - (\boldsymbol{\omega}^I \cdot \nabla)\boldsymbol{U} - (\boldsymbol{\Omega} \cdot \nabla)\boldsymbol{u}^I + (\boldsymbol{u} \cdot \nabla)\boldsymbol{\omega} - (\boldsymbol{\omega} \cdot \nabla)\boldsymbol{u} + \nabla \Psi] \mathrm{d}V. \tag{25}$$

Before proceeding with the analysis, the role of the artificially superposed potential vorticity, $\nabla \Psi(\boldsymbol{x}, t)$, in the evolution of the concentrated vorticity field should be further clarified. – As is shown in Appendix A, the fluid impulse integral of any potential vorticity field is identically zero, provided the integral is taken over a spherical domain. As such, the artificial superposed potential vorticity field $\nabla \Psi(\boldsymbol{x}, t)$ has no direct impact on the impulse evolution of the concentrated vorticity $\boldsymbol{\omega}^I(\boldsymbol{x}, t)$, i.e.

$$\int_{|\boldsymbol{x}| \leqslant R_1} \boldsymbol{x} \times \nabla \Psi(\boldsymbol{x}, t) \mathrm{d}V \equiv 0. \tag{26}$$

On the other hand, the potential vorticity, $\nabla \Psi(\boldsymbol{x}, t)$, is the only driving force associated with the vorticity field, $\boldsymbol{\omega}^{II}(\boldsymbol{x}, t)$, which initially is zero everywhere. Since $\Psi_i(\boldsymbol{x}, t)$ is a harmonic function, it attains its maximum on the boundary $R > \delta$. Consequently, using (22), the magnitude of the generated vorticity is estimated to be $|\boldsymbol{\omega}^{II}| \sim |\boldsymbol{p}|/R^4$ for times of $O(1/|\boldsymbol{\Omega}|)$. However, since within the domain $|\boldsymbol{x}| \leqslant R$, lines of constant $\nabla \Psi$ are at most linear with $\boldsymbol{x}$ (see (22)), they cannot be enclosed within the disturbed region and therefore this field of vorticity cannot be associated with the concentrated vorticity region, which we intend to follow. Moreover, based on experimental observations, in most cases the concentrated vorticity is confined within a small filament having a hairpin or horseshoe shape. Their length is relatively small, of $O(\delta)$, whereas their typical cross-section diameter is of order $\delta_1 \ll \delta$. Therefore, the magnitude of the fluid impulse in this case is $|\boldsymbol{p}| = O(|\boldsymbol{\omega}^I| \delta^2 \delta_1^2)$. Thus, the ratio $|\boldsymbol{\omega}^{II}|/|\boldsymbol{\omega}^I|$ within the region $|\boldsymbol{x}| \leqslant R$ is at most proportional to δ_1^2/δ^2.

We now return to the analysis. The detailed evaluation of the integrals on the right-hand side of (25) is given in Appendix A. Accordingly, the time evolution of the fluid impulse, written in a vector form, is given by the following equation:

$$\frac{\mathrm{d}\boldsymbol{p}}{\mathrm{d}t} = -\nabla(\boldsymbol{p} \cdot \boldsymbol{U}) - \tfrac{1}{2}\boldsymbol{\Omega}(0) \times \boldsymbol{p}, \tag{27}$$

in which the vector $\boldsymbol{U}$ corresponds only to the leading term of (6). Equivalently, by using the relation $\boldsymbol{\Omega} = \nabla \times \boldsymbol{U}$, one can obtain

$$\frac{\mathrm{d}\boldsymbol{p}}{\mathrm{d}t} = -\tfrac{1}{2}\nabla(\boldsymbol{p} \cdot \boldsymbol{U}) - \tfrac{1}{2}(\boldsymbol{p} \cdot \nabla)\boldsymbol{U}, \tag{28}$$

where the derivatives of $\boldsymbol{U}$ are to be evaluated at $\boldsymbol{x} = 0$.

Finally, it should be noted that although viscosity plays a crucial role in the generation of the initial localized disturbance, it plays no role in equation (27) which describes the evolution of the fluid impulse. In fact, if one includes the viscosity term, $\nu\Delta\boldsymbol{\omega}$ in (20), its corresponding additional integral in (25) is zero since it may be transformed to surface integrals, which vanish in view of the asymptotic behaviour of the vorticity ($|\boldsymbol{\omega}| \sim |\boldsymbol{x}|^{-4}$) far from the origin.

3. Application to two representative examples

3.1. *Application to plane parallel shear flows and boundary layers*

For a parallel plane shear flow the external velocity field is given by $\boldsymbol{U} = (U(y), 0, 0)$, for which a right-handed coordinate system is used with $\boldsymbol{x} = (x, y, z)$, where the vector entries are the downstream, vertical (wall-normal) and spanwise directions, respectively. This external field can also be regarded as a very good approximation for a high Reynolds number two-dimensional boundary layer. For such cases the impulse vector equation (28) is reduced to

$$\frac{\mathrm{d}p_x}{\mathrm{d}t} = -\tfrac{1}{2}p_y\frac{\mathrm{d}U}{\mathrm{d}y}, \quad \frac{\mathrm{d}p_y}{\mathrm{d}t} = -\tfrac{1}{2}p_x\frac{\mathrm{d}U}{\mathrm{d}y}, \quad \frac{\mathrm{d}p_z}{\mathrm{d}t} = 0, \tag{29a–c}$$

where $\boldsymbol{p} = (p_x, p_y, p_z)$. The general solution of (29) is

$$p_x = -\frac{p_y(0)-p_x(0)}{2}\exp\left(\frac{1}{2}\frac{\mathrm{d}U}{\mathrm{d}y}t\right)+\frac{p_y(0)+p_x(0)}{2}\exp\left(-\frac{1}{2}\frac{\mathrm{d}U}{\mathrm{d}y}t\right), \tag{30a}$$

$$p_y = \frac{p_y(0)-p_x(0)}{2}\exp\left(\frac{1}{2}\frac{\mathrm{d}U}{\mathrm{d}y}t\right)+\frac{p_y(0)+p_x(0)}{2}\exp\left(-\frac{1}{2}\frac{\mathrm{d}U}{\mathrm{d}y}t\right), \tag{30b}$$

$$p_z = p_z(0), \tag{30c}$$

where $p_x(0)$, $p_y(0)$ and $p_z(0)$ are the initial fluid impulse components at $t = t_0$. The solution (30) implies that any inviscid two-dimensional plane shear flow is unstable to a three-dimensional localized disturbance.

For times much greater than $(\mathrm{d}U/\mathrm{d}y)^{-1}$, the exponentially growing terms in (30) become dominant and consequently the solution for the fluid impulse can be approximated as

$$p_x = -p_y = -C_0\exp\left(\tfrac{1}{2}(\mathrm{d}U/\mathrm{d}y)\,t\right), \tag{31}$$

where the constant C_0, which is determined from the initial vorticity distribution, is positive for positive values of the vertical component of the fluid impulse. According to the solution (31), $\boldsymbol{p}$ is aligned to the flow direction at 135°. Since the fluid impulse vector is perpendicular to the plane of any vortex dipole such as the hairpin one, the latter is predicted to be inclined to the flow direction at an angle of 45°, regardless of its initial vorticity distribution, $\boldsymbol{\omega}_0(\boldsymbol{x})$. Within the limits of experimental error, this is exactly the characteristic angle observed by Head & Bandyopadhyay (1981) in a turbulent boundary layer and by Acarlar & Smith (1987*a*, *b*) in a laminar boundary layer. To the best of our knowledge, the only previous analytical attempt to predict the 45° inclination angle, was done by Theoderson in 1952. According to his arguments, the material derivative of $\boldsymbol{\omega}\cdot\boldsymbol{\omega}$ is proportional to the stretching term $\omega_x\omega_y(\partial U/\partial y)$, and the latter will be maximum when the component of the vorticity vector is inclined at 45° to the main flow direction, in a plane normal to the transverse axis. However, this is not a satisfactory explanation since, as was pointed by Head & Bandyopadhyay (1981),

the question as to why the hairpin vortices should set themselves at the angle which makes the contribution of the stretching term maximum still remains unanswered.

The set of two linear coupled equations (29*a*, *b*) describes a simple feedback mechanism in which the growth of one component of the fluid impulse enhances the growth of the other and vice versa. The dynamics of the localized vorticity disturbance associated with these two coupled equations can be explained, in view of equation (25), as follows: the liftup of the disturbance in the vertical direction stretches the external spanwise vorticity field and generates a disturbed vorticity component in the vertical direction, which is equivalent to a further growth of the streamwise component of the fluid impulse. The direct effect of the external shear flow is to rotate the disturbed vortex back towards the wall and thereby to amplify the streamwise vorticity component as well as the vertical component of the fluid impulse. The new streamwise vorticity component generated induces an additional vertical velocity which further enhances the liftup effect and closes the feedback loop. Hence, the inclination of the hairpin vortices at 45° is a result of two conflicting effects: the liftup effect caused by the vertical induced motion on the one hand and the stretching and tilting due to the external shear on the other.

The above scenario is similar but not equivalent to the one suggested by Head & Bandyopadhyay (1981) and elaborated by Acarlar & Smith (1987*a*). According to them, the shear effect is opposed by the induced velocity that each leg of the hairpin imposes upon the other. We on the other hand emphasize the importance of the integrated vertical liftup effect, according to which a major part of the horizontal momentum is retained when a low-speed fluid particle is vertically displaced. This process is accompanied by the generation of vertical vorticity in the disturbed vortical region and its surroundings. The success of this analysis in predicting the inclination angle of the hairpin vortices is clearly due to the use of the fluid impulse which accounts for the *integral character* of the liftup effect. Universality expresses itself in the 45° angle of inclination of the hairpin vortices regardless of the details of the flow (magnitude and shape of the external velocity shear, initial distribution of the disturbed vorticity and Reynolds number).

Since nonlinearity is included in the analysis, the growth of the fluid impulse in parallel shear flows is moderated only by the growth of the disturbance geometrical scale which invalidates the assumption that $\delta/\Delta \ll 1$. If one were to include the next higher-order terms in the Taylor series expansions (6) and (7) then the right-hand side of (A 1), which describes the time evolution of the fluid impulse in tensor notation, would include terms like

$$\epsilon_{ijk} \frac{\partial^2 U_k}{\partial x_l \partial x_m} \int \omega_l^I x_m x_j \, \mathrm{d}V.$$

The asymptotic forms of these terms require the consideration of additional terms in (13) and (18) to ensure that these integrals are absolutely convergent. For a general initial vorticity distribution, these integrals cannot be evaluated analytically, but it is a straightforward procedure to estimate them to be $O(\delta/\Delta)$ smaller than the leading terms.

3.2. *Application to the Taylor–Couette flow*

In order to facilitate a careful examination of the model we developed a new instability criterion, associated with finite-amplitude three-dimensional localized disturbances, for the relatively simple Taylor–Couette flow, which, however, has some additional dynamical effects owing to rotation.

3.2.1. *Theoretical considerations*

The stability of external stationary circular flows of an incompressible fluid between two infinite long rotating coaxial cylinders to localized disturbances is considered here. The radii of the inner and outer cylinders are R_i and R_o, respectively, and Ω_i and Ω_o denote the angular velocity of rotation about the axis of the two cylinders. In cylindrical polar coordinates r, ϕ, z, the external velocity field is given by $\boldsymbol{U} = (U_r, U_\phi, U_z) = (0, V(r), 0)$, where

$$V(r) = Ar + B/r, \tag{32}$$

for which the constants A and B are

$$A = \frac{\Omega_o R_o^2 - \Omega_i R_i^2}{R_o^2 - R_i^2} \quad \text{and} \quad B = \frac{(\Omega_i - \Omega_o) R_o^2 R_i^2}{R_o^2 - R_i^2}. \tag{33}$$

The corresponding external vorticity field is $\boldsymbol{\Omega} = \nabla \times \boldsymbol{U} = (\Omega_r, \Omega_\phi, \Omega_z) = (0, 0, \Omega)$, where $\Omega = 2(\Omega_o R_o^2 - \Omega_i R_i^2)/(R_o^2 - R_i^2)$.

We examine the possibility of the external flow being subjected to a three-dimensional localized disturbance, which is positioned at a radial distance $r = r_d$ between the two cylinders so that $R_i \leqslant r_d \leqslant R_o$. In order to follow the disturbed region, we change from the laboratory frame to a frame attached to the disturbance and rotating with it, at an angular velocity $\Omega_d = V(r_d)/r_d$. In the new rotating frame, the external flow variables are denoted by a tilde. Accordingly, the expressions for the external velocity and vorticity are

$$\tilde{\boldsymbol{U}} = (0, V - \Omega_d r, 0) \quad \text{and} \quad \tilde{\boldsymbol{\Omega}} = (0, 0, \Omega - 2\Omega_d), \tag{34}$$

whereas the vorticity equation (10) is given by

$$\frac{\partial \boldsymbol{\omega}}{\partial t} + (\tilde{\boldsymbol{U}} \cdot \nabla)\boldsymbol{\omega} - (\boldsymbol{\omega} \cdot \nabla)\tilde{\boldsymbol{U}} + (\boldsymbol{u} \cdot \nabla)\boldsymbol{\omega} - (\boldsymbol{\omega} \cdot \nabla)\boldsymbol{u} - (\tilde{\boldsymbol{\Omega}} \cdot \nabla)\boldsymbol{u} - 2(\boldsymbol{\Omega}_d \cdot \nabla)\boldsymbol{u} = 0, \tag{35}$$

where the last term represents the Coriolis force which occurs when the fluid has a motion relative to the rotating coordinates, and $\boldsymbol{\Omega}_d = (0, 0, \Omega_d)$.

In order to obtain the time evolution of the fluid impulse of the disturbance we follow the same procedure described in §2. In fact one can skip all the details and substitute $\tilde{\boldsymbol{U}}$ and $\tilde{\boldsymbol{\Omega}} + 2\boldsymbol{\Omega}_d$ instead of $\boldsymbol{U}$ and $\boldsymbol{\Omega}$ in (27), respectively, to obtain

$$\frac{\mathrm{d}\boldsymbol{p}}{\mathrm{d}t} = -\nabla(\boldsymbol{p} \cdot \tilde{\boldsymbol{U}}) - \tfrac{1}{2}(\tilde{\boldsymbol{\Omega}} + 2\boldsymbol{\Omega}_d) \times \boldsymbol{p}, \tag{36}$$

where the external flow variables are evaluated at r_d. Substituting (34) into (36) yields the following system of linear equations:

$$\frac{\mathrm{d}p_r}{\mathrm{d}t} = p_\phi \left(A + 2\frac{B}{r_d^2} \right), \quad \frac{\mathrm{d}p_\phi}{\mathrm{d}t} = -Ap_r, \quad \frac{\mathrm{d}p_z}{\mathrm{d}t} = 0, \tag{37a–c}$$

for which the eigenvalues $\{\lambda_i\}_{i=1}^3$ can be found from the characteristic equation

$$\lambda_i \left[\lambda_i^2 + A\left(A + 2\frac{B}{r_d^2} \right) \right] = 0. \tag{38}$$

Hence, the flow under investigation is stable with respect to three-dimensional localized disturbances only if the real part of λ_i is not positive. Therefore, for stability we require that

$$A\left(A+2\frac{B}{r_d^2}\right) \geqslant 0, \tag{39}$$

or

$$(\Omega_o R_o^2-\Omega_i R_i^2)\left[(\Omega_o R_o^2-\Omega_i R_i^2)+\frac{2(\Omega_i-\Omega_o) R_o^2 R_i^2}{r_d^2}\right] \geqslant 0, \tag{40}$$

where (33) is substituted into (39).

A complete stability analysis is given in Appendix B. A detailed comparison between the theoretical results of Appendix B and experiments requires a sophisticated flow-visualization technique for a Taylor–Couette apparatus where both cylinders can be rotated independently. This experimental facility is under construction at the moment and thus only experimental results corresponding to the case in which the inner cylinder is fixed, will be presented here. Under these conditions, the flow is known to be stable to any axisymmetrical disturbance as predicted by the Rayleigh inviscid criterion. The Landau & Lifshitz (1959) generalization of the Rayleigh criterion predicts stability of this flow to any three-dimensional disturbance. This result stands in contradiction to the present calculations. According to these, if Ω_i is set to zero in (40), one obtains that stability occurs if

$$r_d \geqslant \sqrt{2}\, R_i. \tag{41}$$

For $r_d = R_i$, as an example, the above inequality implies that the flow is unstable to any three-dimensional localized disturbance. The source of the disagreement between the two criteria is that the motion induced by the disturbance as it is displaced radially is considered as an essential part of the feedback mechanism described above, whereas it was completely ignored in the calculation of Landau & Lifshitz (1959).

3.2.2. *Preliminary experimental results*

A Taylor–Couette apparatus consisting of a stationary circular cylinder inside a concentrically rotating outer cylinder, and using water as a working fluid, was constructed for this investigation. Hairpin vortices were generated at the inner cylinder using an injection–suction technique with coloured water. Pictures of the flow were taken with a Hi 8 mm video camera. A schematic drawing of the side view assembly of the Taylor–Couette experiment is shown in figure 1.

The inner cylinder consisted of a stainless steel tube, 850 mm long, having an outer diameter of 101 ± 0.1 mm and a thickness of 5 mm. This cylinder was kept fixed in place using a break. The outer cylinder was a Plexiglas tube, 800 mm long, with an inner diameter of 190 ± 1 mm and a thickness of 10 mm. These dimensions were chosen so that an initial disturbed region, having a typical dimension of 5 mm, could be considered small in comparison with the spatial scale of the external flow field. The diameters of the two cylinders need not be precisely controlled, since only local effects were investigated. The cylinders were supported at both ends by ball bearings. The rotation of the outer cylinder was driven by a controlled variable-speed electric motor, which was connected to the bottom ball bearing through a worm gear unit and a 'V' belt. For the present investigation the outer cylinder was rotated at a constant angular velocity of 60 r.p.m.

In order to facilitate the injection of dye, a horizontal plate was mounted on the top end of the inner cylinder. This plate served as a stand for a dye injection unit and a low-

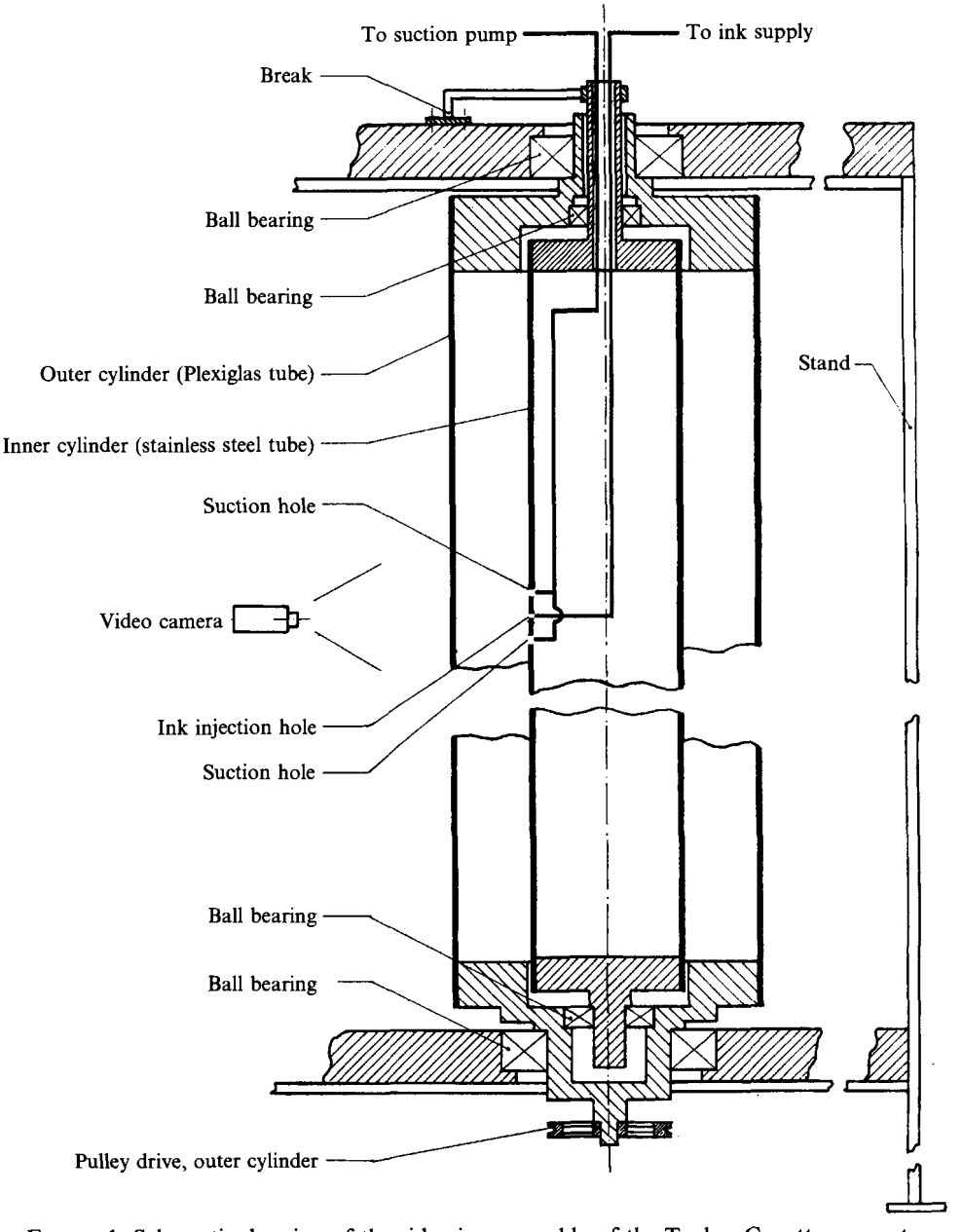

FIGURE 1. Schematic drawing of the side-view assembly of the Taylor–Couette apparatus.

vacuum pump which were placed on it. The injection unit consisted of a 2 l pressurized reservoir filled with coloured water. The dye was injected normal to the cylinder wall through a small hole of diameter 0.8 mm. To assure that the results were independent of the hole location, several holes located at different heights of the cylinder were used alternately. The coloured water flowed slowly from the dye injection unit to one of the holes through a capillary, positioned inside the inner cylinder. The rate of the dye flow was monitored by a flow control valve. Two additional small holes of 2 mm in diameter were located 5 mm above and below the dye injection hole along the cylinder axis. These holes served for suction of water around the injection area. The holes were connected to the vacuum pump through two tubes, which ran inside the inner cylinder

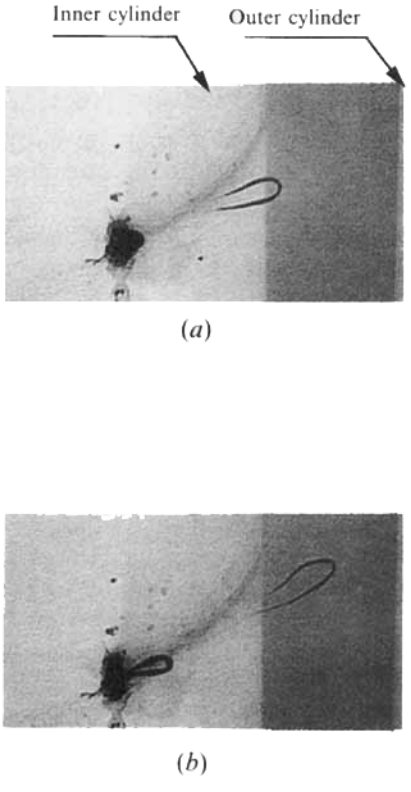

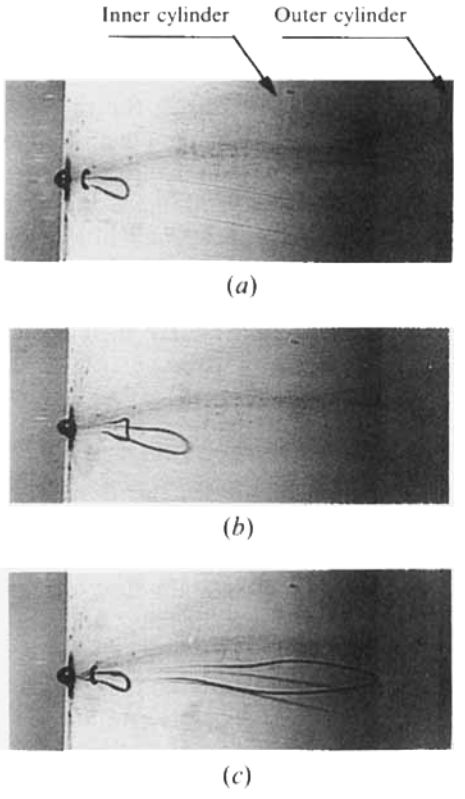

FIGURE 2

FIGURE 3

FIGURE 2. Time-sequence visualization (downstream view) of the hairpin vortex evolution. External flow is from left to right. The large black spot on the left corresponds to the region of the initial disturbance.

FIGURE 3. Time-sequence visualization (upstream view) of the hairpin vortex evolution. External flow is from left to right.

and passed through a flow control valve. By adjusting the ratio between the dye injection and the suction applied through the two side holes, a distinguishable initial localized vortex disturbance was generated, having a typical size of 5 mm.

A time sequence of two side-view visualizations of hairpin vortices is presented in figure 2, wherein the direction of the external flow is from left to right (counterclockwise). A single hairpin vortex just after it was released from the dye injection region (the black spot upstream of it) is shown in figure 2(*a*). The growth of the vortex as it travels downstream and the birth of a second vortex are clearly evident in the bottom picture (figure 2*b*), which was taken a short time later. Moreover, the radial development of the vortex away from the sidewall of the inner cylinder can be seen from this figure.

Another view of the vortex formation is given by the time sequence of end-view visualizations (looking upstream), displayed in figure 3. The black spot on the left side of the inner cylinder is the injection–suction region (the source of the three-dimensional disturbance). Slightly to the right there is a structure which is composed of two parts: the left part (which is darker) is the hairpin itself, while the longer loop extending to the right is its shadow. As before, the formation of a single hairpin vortex is observed just downstream of the dye injection region. Owing to the lighting angle, the vortex

itself appears to be much smaller than its shadow. The growth of the hairpin vortex at later times is shown in the next two pictures (figures 3*b* and 3*c*).

The vortex structures observed in the present experiments are very similar to the ones found by Acarlar & Smith (1987*a*, *b*) and by Hagen & Kurosaka (1993) in a laminar boundary layer, even though the methods used in generating the hairpin vortices were not exactly the same. In their experiments, relatively long streamwise slots were used for fluid injection, whereas we used a combination of dye injection and suction through three small holes positioned at the same streamwise location. This agrees with our conclusion that the growth of the localized vortical disturbances is independent of their initial distributions. Furthermore, the evolution of the hairpin vortices, and in particular their radial growth, strongly support the new instability criteria described above.

4. Summary and conclusions

A model which uses the fluid impulse as an integral characteristic of localized disturbances embedded in external shear flows has been developed. According to its predictions, such initial disturbances, in plane shear flows, are amplified exponentially and inclined to the main flow direction at 45°, regardless of their initial vorticity distribution. These results are in full agreement with previous experimental observations. The instability mechanism is an inviscid one and consists of two conflicting effects: the first is the generation of vertical vorticity caused by the vertical displacement of the vortex and its surroundings, whereas the second effect is the generation of horizontal vorticity due to the rotation of the disturbed vortex by the external shear flow.

Knowledge of the amplitude of the initial disturbance is not a prerequisite of the model, since the contribution of nonlinear effects to the evolution of the fluid impulse integral is zero. This does not mean that nonlinearity is not important. On the contrary, we think that strong and local nonlinear effects are essential for forming vortical structures such as the hairpin ones. The present analysis does not account for such local nonlinear effects and therefore cannot explain why hairpin or horseshoe shapes are formed. However, the subdivision used in the analysis of the vorticity field into a bounded near field, ω^I, and far-field vorticity tails, ω^{II}, induced by the integrated liftup effect, relies upon the existence of such vortical configurations.

The theoretical approach taken in this investigation is of a general nature and can be applied to various shear flows. Its application to Taylor–Couette flow, which has some additional dynamical effects owing to rotation, reveals a new instability criterion associated with three-dimensional localized disturbances. The validity of this criterion is supported by present experimental results. According to these, hairpin structures similar to the ones observed in a laminar boundary layer were found for conditions under which the flow is predicted to be stable according to the Landau & Lifshitz criterion.

The authors would like to thank A. Beer for his help in designing and building the apparatus and carrying out the experiments. The authors are also grateful to D. Katzen for his careful reading of the manuscript and helpful discussion. The research was supported by Grant No. 3875-2-93 from the Israeli Ministry of Science and Technology and by Technion V.P.R. Fund – Albert Fund for R. and D. Aer. Eng.

Appendix A

The purpose of this appendix is to evaluate the integrals on the right-hand side of (25). It is convenient to introduce a Cartesian tensor notation, i.e.

$$\begin{aligned}\frac{\mathrm{d}p_i}{\mathrm{d}t} &= \lim_{R_1\to\infty}\left[\frac{1}{2}\int_{|x|\leqslant R_1}\epsilon_{ijk}x_j\left(-U_t\frac{\partial\omega_k^I}{\partial x_t}+\omega_l^I\frac{\partial U_k}{\partial x_l}\right)\mathrm{d}V+\frac{1}{2}\int_{|x|\leqslant R_1}\epsilon_{ijk}x_j\Omega_l\frac{\partial u_k^I}{\partial x_l}\mathrm{d}V\right.\\ &\quad\left.+\frac{1}{2}\int_{|x|\leqslant R_1}\epsilon_{ijk}x_j\left(-u_l\frac{\partial\omega_k}{\partial x_l}+\omega_l\frac{\partial u_k}{\partial x_l}\right)\mathrm{d}V-\frac{1}{2}\int_{|x|\leqslant R_1}\epsilon_{ijk}x_j\frac{\partial\Psi}{\partial x_k}\mathrm{d}V\right]\\ &= \lim_{R_1\to\infty}(I_1+I_2+I_3+I_4),\end{aligned}\tag{A 1}$$

where ϵ_{ijk} is the alternating tensor and the usual summation convention is applied.

We shall evaluate each one of the integrals, I_1-I_4, for a finite value of R_1 and then take their limits as $R_1\to\infty$.

The integral I_1 is given by

$$I_1=\frac{1}{2}\int_{|x|\leqslant R_1}\epsilon_{ijk}x_j\left(-U_t\frac{\partial\omega_k^I}{\partial x_t}+\omega_l^I\frac{\partial U_k}{\partial x_l}\right)\mathrm{d}V.\tag{A 2}$$

In order to evaluate the integral of the first term in (A 2), we first use integration by parts and then employ Gauss' divergence theorem and use the incompressible continuity equation for the external flow. Thus,

$$-\tfrac{1}{2}\epsilon_{ijk}\int_{|x|\leqslant R_1}x_j\,U_t\frac{\partial\omega_k^I}{\partial x_t}\mathrm{d}V=\tfrac{1}{2}\epsilon_{ijk}\,\delta_{tj}\int_{|x|\leqslant R_1}U_t\,\omega_k^I\,\mathrm{d}V-\tfrac{1}{2}\epsilon_{ijk}\oint_{|x|=R_1}n_t\,x_j\,U_t\,\omega_k^I\,\mathrm{d}S,\tag{A 3}$$

where $\boldsymbol{n}$ is a unit vector normal to the sphere surface.

In accordance with the order of magnitude estimations (see §2), we use the first term of the Taylor series expansion (6) to approximate the external velocity so that

$$I_1=\frac{1}{2}\int_{|x|\leqslant R_1}\epsilon_{ijk}\left(\omega_k^I\,x_l\frac{\partial U_j(0)}{\partial x_l}+\omega_l^I\,x_j\frac{\partial U_k(0)}{\partial x_l}\right)\mathrm{d}V-\frac{1}{2}\oint_{|x|=R_1}\epsilon_{ijk}\,n_t\,x_j\,x_l\frac{\partial U_t(0)}{\partial x_l}\omega_k^I\,\mathrm{d}S.\tag{A 4}$$

By permutating the indexes j and k in the first term of the volumetric integral in (A 4) we obtain

$$I_1=\tfrac{1}{2}\epsilon_{ijk}\frac{\partial U_k(0)}{\partial x_l}\int_{|x|\leqslant R_1}(\omega_l^I\,x_j-\omega_j^I\,x_l)\,\mathrm{d}V-\tfrac{1}{2}\epsilon_{ijk}\frac{\partial U_t(0)}{\partial x_l}\oint_{|x|=R_1}n_t\,x_j\,x_l\,\omega_k^I\,\mathrm{d}S,\tag{A 5}$$

which in the limit $R_1\to\infty$, where the asymptotic expression (23) for $\boldsymbol{\omega}^I$ is valid, yields the neglect of the surface integral in (A 5). Consequently,

$$\lim_{R_1\to\infty}I_1=\tfrac{1}{2}\epsilon_{ijk}\frac{\partial U_k(0)}{\partial x_l}\int(\omega_l^I\,x_j-\omega_j^I\,x_l)\,\mathrm{d}V.\tag{A 6}$$

In order to evaluate this integral, we rewrite the expression for the fluid impulse using tensor notation, i.e.

$$p_t=\tfrac{1}{2}\epsilon_{tmn}\int x_m\,\omega_n^I\,\mathrm{d}V.\tag{A 7}$$

Multiplying the fluid impulse by the alternating tensor ϵ_{tlj} and using the identity $\epsilon_{tlj}\epsilon_{tmn}=\delta_{lm}\,\delta_{jn}-\delta_{ln}\,\delta_{jm}$, where δ_{ij} is the Kronecker delta function, yields

$$\epsilon_{tlj}p_t=-\frac{1}{2}\int(\omega_l^I\,x_j-\omega_j^I\,x_l)\,\mathrm{d}V.\tag{A 8}$$

Substituting (A 8) into (A 6) and using once again the identity mentioned above, the final expression for I_1 can be written as

$$\lim_{R_1\to\infty} I_1 = -p_k \frac{\partial U_k(0)}{\partial x_i}. \tag{A 9}$$

The evaluation of I_2 follows a similar procedure. Accordingly, we use integration by parts and employ Gauss' divergence theorem and Taylor series expansion to obtain

$$\begin{aligned} I_2 &= \frac{1}{2}\int_{|x|\leqslant R_1} \epsilon_{ijk} x_j \Omega_l \frac{\partial u_k^I}{\partial x_l} \mathrm{d}V \\ &= \tfrac{1}{2}\epsilon_{ijk}\Omega_l(0)\oint_{|x|=R_1} n_l x_j u_k^I \,\mathrm{d}S - \tfrac{1}{2}\epsilon_{ijk}\Omega_j(0)\int_{|x|\leqslant R_1} u_k^I \,\mathrm{d}V = I_{21}+I_{22}. \end{aligned} \tag{A 10}$$

In order to calculate the first integral I_{21}, a similar expression to (13) is used to describe the asymptotic far-field behaviour of $\boldsymbol{u}^I$. Thus,

$$I_{21} = \tfrac{1}{2}\epsilon_{ijk}\Omega_l(0)\oint_{|x|=R_1} n_l x_j \left\{\left(-\frac{1}{4\pi}\right)\left[\frac{p_k}{|x|^3} - \frac{3(\boldsymbol{p}\cdot\boldsymbol{x})x_k}{|x|^5}\right] + O\left(\frac{1}{|x|^4}\right)\right\}\mathrm{d}S, \tag{A 11}$$

which in the limit $R_1\to\infty$ is reduced to

$$\lim_{R_1\to\infty} I_{21} = -\frac{1}{8\pi}\epsilon_{ijk}\Omega_l(0)\int_0^{2\pi}\mathrm{d}\phi\int_0^{\pi}\sin(\theta)\,\mathrm{d}\theta[n_l n_j(p_k - 3p_t n_t n_k)]. \tag{A 12}$$

A straightforward calculation of (A 12) using the symmetry properties of the alternating tensor yields

$$\lim_{R_1\to\infty} I_{21} = -\tfrac{1}{6}\epsilon_{ijk}\Omega_j(0)p_k. \tag{A 13}$$

It is convenient to write the second integral I_{22} as

$$I_{22} = -\tfrac{1}{2}\epsilon_{ijk}\Omega_j(0)J_k, \tag{A 14}$$

where J_k is given by

$$J_k = \int_{|x|\leqslant R_1} u_k^I(x)\,\mathrm{d}V. \tag{A 15}$$

Using the relation (16), in tensor notation, and changing the order of integration yields

$$J_k = \frac{1}{4\pi}\epsilon_{klm}\int \mathrm{d}V'\,\omega_m^I(x')\int_{|x|\leqslant R_1}\frac{(x_l'-x_l)}{|x'-x|^3}\mathrm{d}V. \tag{A 16}$$

The integral on the right is well known from potential theory; for example it represents the electrostatic field due to a sphere of radius R_1 uniformly filled with space charge of unit density. The result of this integral is

$$\int_{|x|\leqslant R_1}\frac{(x_l'-x_l)}{|x'-x|^3}\mathrm{d}V = \begin{cases} 4\pi x_l'/3 & |x'|\leqslant R_1 \\ 4\pi R_1^3 x_l'/(3|x'|^3), & |x'|>R_1. \end{cases} \tag{A 17}$$

Substitution of (A 17) into (A 16) yields

$$J_k = \tfrac{1}{3}\epsilon_{klm}\int_{|x'|\leqslant R_1} x_l'\,\omega_m^I(x')\,\mathrm{d}V' + \frac{R_1^3}{3}\epsilon_{klm}\int_{|x'|>R_1}\frac{x_l'\,\omega_m^I(x')}{|x'|^3}\mathrm{d}V'. \tag{A 18}$$

Taking the limit $R_1 \to \infty$ and using the asymptotic expression (23) for ω^I we obtain that the second integral of (A 18) vanishes and consequently

$$\lim_{R_1 \to \infty} J_k = \tfrac{2}{3} p_k, \tag{A 19}$$

where the definition of fluid impulse (A 7) was used. Using (A 19), the limit of I_{22} as $R_1 \to \infty$ is given by

$$\lim_{R_1 \to \infty} I_{22} = -\tfrac{1}{3} \epsilon_{ijk} \Omega_j(0) p_k, \tag{A 20}$$

which together with I_{21} results in

$$\lim_{R_1 \to \infty} I_2 = -\tfrac{1}{2} \epsilon_{ijk} \Omega_j(0) p_k. \tag{A 21}$$

The integral I_3, which is given by

$$I_3 = \frac{1}{2} \int_{|x| \leqslant R_1} \epsilon_{ijk} x_j \left(-u_l \frac{\partial \omega_k}{\partial x_l} + \omega_l \frac{\partial u_k}{\partial x_l} \right) \mathrm{d}V, \tag{A 22}$$

represents the evolution of the fluid impulse due to the nonlinear self-induced motion of the disturbed field. This integral tends to zero as $R_1 \to \infty$ (Batchelor 1967).

Finally the integral I_4 which represents the evolution of the fluid impulse due to the artificial superposed potential vorticity field is evaluated. Integration by parts and using Gauss' divergence theorem yields

$$I_4 = -\tfrac{1}{2} \epsilon_{ijk} \int_{|x| \leqslant R_1} x_j \frac{\partial \Psi}{\partial x_k} \mathrm{d}V = -\tfrac{1}{2} \epsilon_{ijk} \oint_{|x| = R_1} n_k x_j \Psi \mathrm{d}S + \tfrac{1}{2} \epsilon_{ijk} \delta_{jk} \int_{|x| \leqslant R_1} \Psi \mathrm{d}V. \tag{A 23}$$

Using the properties of the alternating and symmetrical tensors $\epsilon_{ijk} \delta_{jk} \equiv 0$, and $\epsilon_{ijk} n_k n_j \equiv 0$, it immediately follows that $I_4 \equiv 0$.

The substitution of (A 9) and (A 21) into (A 1) together with the results that $\lim_{R_1 \to \infty}(I_3) = I_4 = 0$ yields

$$\frac{\mathrm{d}p_i}{\mathrm{d}t} = -p_k \frac{\partial U_k(0)}{\partial x_i} - \tfrac{1}{2} \epsilon_{ijk} \Omega_j(0) p_k, \tag{A 24}$$

which in a vector form is given by

$$\frac{\mathrm{d}\boldsymbol{p}}{\mathrm{d}t} = -\nabla(\boldsymbol{p} \cdot \boldsymbol{U}) - \tfrac{1}{2} \boldsymbol{\Omega}(0) \times \boldsymbol{p}, \tag{A 25}$$

where it is understood that

$$\boldsymbol{U}(\boldsymbol{x}) = \sum_{j=1}^{3} \frac{\partial \boldsymbol{U}(0)}{\partial x_j} x_j. \tag{A 26}$$

Appendix B

The purpose of this Appendix is to analyse the criteria for stability of Taylor–Couette flow to a three-dimensional localized disturbance (40), with respect to its position r_d and the non-dimensional parameters R_o/R_i and Ω_o/Ω_i. We begin with the criterion obtained in §3, according to which the flow is stable if

$$(\Omega_o R_o^2 - \Omega_i R_i^2)[\Omega_o R_o^2 - \Omega_i R_i^2 + 2(\Omega_i - \Omega_o) R_o^2 R_i^2 / r_d^2] \geqslant 0. \tag{B 1}$$

Without loss of generality we set $\Omega_o > 0$. For $\Omega_i < 0$, expression (B 1) can be written as

$$(\Omega_o R_o^2 + |\Omega_i| R_i^2)[\Omega_o R_o^2 + |\Omega_i| R_i^2 - 2(|\Omega_i| + \Omega_o) R_o^2 R_i^2 / r_d^2] \geqslant 0, \tag{B 2}$$

which is equivalent to

$$\Omega_o R_o^2 (r_d^2 - 2R_i^2) \geqslant |\Omega_i| R_i^2 (2R_o^2 - r_d^2). \tag{B 3}$$

Hence, the flow is unstable for $r_d < \sqrt{2}\, R_i$ and is stable for $r_d \geqslant \sqrt{2}\, R_i$ and

$$|\Omega_i| \leqslant \Omega_o \frac{R_o^2}{R_i^2} \frac{r_d^2 - 2R_i^2}{2R_o^2 - r_d^2}. \tag{B 4}$$

Thus, for a narrow-gap apparatus so that $R_o/R_i < \sqrt{2}$ the flow is always unstable when the two cylinders rotate in opposite directions.

For $\Omega_i > 0$, we first consider the case where $\Omega_o R_o^2 < \Omega_i R_i^2$. In this case we obtain that the flow is stable only if

$$\Omega_o R_o^2 ((2R_i^2/r_d^2) - 1) \geqslant \Omega_i R_i^2 ((2R_o^2/r_d^2) - 1). \tag{B 5}$$

Since $\Omega_o R_o^2$ is assumed to be less than $\Omega_i R_i^2$ and the relation

$$((2R_i^2/r_d^2) - 1) < ((2R_o^2/r_d^2) - 1) \tag{B 6}$$

holds, the inequality (B 5) cannot be satisfied. Hence, for this case the conditions for instability are the same as predicted by the Rayleigh criterion.

Finally we consider the case where $\Omega_o R_o^2 > \Omega_i R_i^2$, which is in fact the Rayleigh inviscid criterion for stability of axisymmetric disturbances when both cylinders rotate in the same direction. For our model we obtain

$$\Omega_o R_o^2 (2R_i^2 - r_d^2) \leqslant \Omega_i R_i^2 (2R_o^2 - r_d^2). \tag{B 7}$$

Equation (B 7) is satisfied and thus the flow is stable provided the initial position of the localized disturbance $r_d \geqslant \sqrt{2}\, R_i$. However, for $r_d < \sqrt{2}\, R_i$ the flow becomes unstable if

$$\Omega_i < \Omega_o \frac{R_o^2}{R_i^2} \frac{2R_i^2 - r_d^2}{2R_o^2 - r_d^2}, \tag{B 8}$$

provided the relation $\Omega_o R_o^2 > \Omega_i R_i^2$ holds. The right-hand side of (B 8) attains a maximum value when $r_d = R_i$. Thus, as the angular velocity of the inner cylinder is decreased below this maximum value, instability, which first occurs in the region adjacent to the inner cylinder, begins.

REFERENCES

Acarlar, M. S. & Smith, C. R. 1987*a* A study of hairpin vortices in a laminar boundary layer. Part 1. Hairpin vortices generated by a hemisphere protuberance. *J. Fluid Mech.* **175**, 1.

Acarlar, M. S. & Smith, C. R. 1987*b* A study of hairpin vortices in a laminar boundary layer. Part 2. Hairpin vortices generated by fluid injection. *J. Fluid Mech.* **175**, 43.

Aref, H. & Flinchem, E. P. 1984 Dynamics of a vortex filament in a shear flow. *J. Fluid Mech.* **148**, 477.

Batchelor, G. K. 1967 *An Introduction to Fluid Dynamics*, pp. 517–520. Cambridge University Press.

Bayly, B. J. 1986 Three-dimensional instability of elliptical flow. *Phys. Rev. Lett.* **57**, 2160.

Bayly, B. J., Orszag, S. A. & Herbert, T. 1988 Instability mechanisms in shear-flow transition. *Ann. Rev. Fluid Mech.* **20**, 359.

BREUER, K. S. & HARITONIDIS, J. H. 1990 The evolution of a localized disturbance in a laminar boundary layer. Part 1. Weak disturbances. *J. Fluid Mech.* **220**, 569.

BREUER, K. S. & LANDAHL, M. T. 1990 The evolution of a localized disturbance in a laminar boundary layer. Part 2. Strong disturbances. *J. Fluid Mech.* **220**, 595.

FARRELL, B. F. & IOANNOU, P. J. 1993 Optimal excitation of three-dimensional perturbations in viscous constant shear flow. *Phys. Fluids* A **5**, 1390.

GRIGORIEV, YU. N., LEVINSKI, V. B., YANENKO, N. N. 1982 Hamiltonian vortex models for turbulence theory. *Chisl. Met. Mech. Spl. Sred.* **13**, No. 3, 13 (in Russian).

GUSTAVSSON, L. H. 1991 Energy growth of three-dimensional disturbances in plane Poiseuille flow. *J. Fluid Mech.* **224**, 241.

HAGEN, J. P. & KUROSAKA, M. 1993 Corewise cross-flow transport in hairpin vortices – the 'tornado effect'. *Phys. Fluids* A **5**, 3167.

HEAD, M. R. & BANDYOPADHYAY, P. 1981 New aspects of turbulent boundary-layers structure. *J. Fluid Mech.* **107**, 297.

HENNINGSON, D. S. 1988 The inviscid initial value problem for a piecewise linear mean flow. *Stud. Appl. Maths* **78**, 31.

HENNINGSON, D. S., LUNDBLADH, A. & JOHANSSON, A. V. 1993 A mechanism for bypass transition from localized disturbances in wall bounded shear flows. *J. Fluid Mech.* **250**, 169.

KLINE, S. J., REYNOLDS, W. C., SCHRAUB, F. A. & RUNSTADLER, P. W. 1967 The structure of turbulent boundary layers. *J. Fluid Mech.* **30**, 741.

LANDAHL, M. T. 1975 Wave breakdown and turbulence. *SIAM J. Appl. Maths* **28**, 735.

LANDAU, L. D. & LIFSHITZ, E. M. 1959 *Fluid Mechanics*, vol. 6, 2nd Edn., pp. 99–100. Pergamon.

MOIN, P. & KIM, J. 1985 The structure of the vorticity field in turbulent channel flow. Part 1. Analysis of instantaneous fields and statistical conditions. *J. Fluid Mech.* **155**, 441.

ORSZAG, S. A. & PATERA, A. T. 1983 Secondary instability of wall-bounded shear flows. *J. Fluid Mech.* **128**, 347.

ROBERTS, P. H. 1972 A Hamiltonian theory for weakly interacting vortices. *Mathematika.* **19**, 169.

ROTT, N. & CANTWELL, B. 1993 Vortex drift. I: Dynamic interpretation. *Phys. Fluids* A **5**, 1443.

RUSSELL, J. M. & LANDAHL, M. T. 1984 The evolution of a flat eddy near a wall in an inviscid shear flow. *Phys. Fluids* **27**, 557.

THEODORSEN, T. 1952 Mechanism of turbulence. *Proc. 2nd Midwestern Conf. on Fluid Mech., Ohio State University.*